

# Learning Temporal Invariance in Android Malware Detectors

Xinran Zheng<sup>1</sup>, Shuo Yang<sup>2</sup>, Edith C.H. Ngai<sup>2</sup>, Suman Jana<sup>3</sup>, and Lorenzo Cavallaro<sup>1</sup>

<sup>1</sup>University College London

<sup>2</sup>University of Hong Kong

<sup>3</sup>Columbia University

## Abstract

Learning-based Android malware detectors degrade over time due to natural distribution drift caused by malware variants and new families. This paper systematically investigates the challenges classifiers trained with empirical risk minimization (ERM) face against such distribution shifts and attributes their shortcomings to their inability to learn *stable* discriminative features. Invariant learning theory offers a promising solution by encouraging models to generate stable representations crossing environments that expose the instability of the training set. However, the lack of prior environment labels, the diversity of drift factors, low-quality representations caused by diverse families make this task challenging. To address these issues, we propose TIF, the first temporal invariant training framework for malware detection, which aims to enhance the ability of detectors to learn stable representations across time. TIF organizes environments based on application observation dates to reveal temporal drift, integrating specialized multi-proxy contrastive learning and invariant gradient alignment to generate and align environments with high-quality, stable representations. TIF can be seamlessly integrated into any learning-based detector. Experiments on a decade-long dataset show that TIF excels, particularly in early deployment stages, addressing real-world needs and outperforming state-of-the-art methods.

## 1 Introduction

In open and dynamic environments, even the most effective malware detectors encounter significant challenges due to natural distribution drift<sup>1</sup>, leading to performance degradation [5, 37]. This degradation arises from the evolution of malware behavior and the emergence of new malware families that detectors have not previously encountered [26]. These

<sup>1</sup>For clarity, we use the terms drift, shift, concept drift/shift, natural drift/shift, and distribution drift/shift interchangeably throughout the text. This is in contrast to adversarial drift or adversarial evasive attacks, which are caused by identifying optimal input perturbations specifically crafted to cause a model’s misclassification.

new variants and families change the underlying statistical properties of the test samples [5, 11, 12, 27], weakening detectors that rely on features derived from past training data, which lack sufficient discriminative power for the new variants [31].

Recent studies have explored incremental training techniques to address distribution drift. These techniques involve detecting new distributions during testing [5, 37] and frequently updating models through active [9, 27] or online learning [6, 19, 36]. However, such approaches incur significant labeling and model update costs. Although pseudo-labeling has been employed to alleviate labeling burdens, it introduces noise that can lead to self-poisoning of models [19, 39], further complicating the learning process. Therefore, enhancing model robustness in drifting scenarios is essential to reduce the frequency of updates. Some studies have attempted static feature augmentation or selecting features that are less sensitive to malware evolution [11, 40, 45]. However, these methods typically require tailored selection strategies for specific feature spaces and depend heavily on the stability of these spaces, limiting their adaptability to diverse drift sources. Ideally, a drift-robust detector should extract invariant features that improve performance and generalize to drifted samples without relying on specific feature space assumptions.

In this paper, we conducted a comprehensive investigation into the brittleness of learning-based malware detectors against natural distribution drift. Our findings indicate that, although invariant features representing shared malicious behaviors exist within malware families or variants, detectors trained using empirical risk minimization (ERM) tend to capture unstable features instead of these invariant ones. This inefficiency arises from the inherent limitations of the ERM training paradigm, which operates under the assumption that training and testing data share the same distribution. ERM typically requires data shuffling or the construction of k-fold cross-validation sets. However, in real-world scenarios, testing data is often collected after the training period [27]. As a result, shuffling the training data disrupts the temporal evolution of malware samples, preventing the model from learning

stable features that persist over time. Consequently, ERM prioritizes unstable features, hindering the model’s adaptability to the dynamic evolution of malware.

Invariant learning theory [8] aims to address the shortcomings of ERM by learning invariant features/representations shared across different distributions, which aligns with our objective. It promotes the discovery of stable representations by dividing training data into distinct subsets or “environments” and encourages the model to minimize differences between them. This is based on two premises: *a priori environment labels that reveal instability* [23, 30] and *high-quality representations that adequately encode feature information* [38]. These assumptions are not trivial for malware detection, as malware evolution is attributed to a variety of non-obvious factors, and the extremely unbalanced sample distributions and complex feature spaces due to multiple malicious families make invariance across environments difficult to explore.

In this paper, we present a Temporal Invariant Training Framework (TIF), for malware detectors to emphasize invariant features under natural distribution drift. TIF firstly partitions training data temporally based on application observation dates, revealing malware evolution without relying on predefined environment labels. Moreover, to model multi-family fused malware categories in binary classification tasks, we propose a multi-proxy contrastive learning module for modular representation learning. While recent study [9] attempts to model positive pairs within each family, such fine-grained approaches exacerbate class imbalance, as smaller families or rare variants may lack adequate representation. Treating multi-family malware categories as homogeneous is also suboptimal due to ignoring detailed patterns in malware families. Our module addresses this by dynamically updating proxies to model subsets within the class, capturing unique patterns within subsets while balancing diversity across subsets and consistency within each subset [24, 41].

TIF further integrates an invariant gradient alignment module to ensure that the encoder produces similar gradients for samples of the same class across environments to enhance temporally invariant representations. Our solution is orthogonal to existing robust malware detectors: it does not rely on new feature spaces, requires no changes to existing model architectures, and can be applied as an enhanced training paradigm to any learning-based detector. The main contributions of this paper are as follows:

- We define invariance in malware evolution, positing that learning discriminative and stable invariant representations is key to mitigating its shortcomings in natural drifting scenarios (Section 3).
- We carefully design multi-proxy contrastive learning (Section 4.4) and invariant gradient alignment (Section 4.5) modules to model and align complex distributions in different temporal environments, encouraging models to learn high-quality and stable representations.

- We present TIF, the first temporal invariant learning framework for malware detectors, which can be integrated with arbitrary learning-based detectors and feature spaces to enhance their ability to learn invariant representations over time by exposing and suppressing unstable information in the drift (Section 4.6).
- We construct a 10-year dataset<sup>2</sup> and a series of experiments to evaluate the robustness of the TIF across various drift scenarios and feature spaces. The results show that TIF effectively slows the detector’s degradation and generates invariant representations that outperform state-of-the-art methods (Section 5).

## 2 Background

In this section, we review the development of malware detectors robust to drift and the key components of invariant learning, laying the groundwork for proposing a temporal invariant representation learning solution tailored for Android malware detection.

### 2.1 Drift-robust Malware Detectors

Existing approaches to enhancing model robustness against drift primarily focus on refining feature representations. One approach identifies features resilient to distribution changes through manual or automated engineering, enabling models to learn patterns less affected by malware evolution [45]. Another approach anticipates future distribution shifts using episode-based learning [29, 42], where pseudo-unknown families are constructed in the training set to simulate low-sample tasks. Each episode replicates a specific learning scenario, fostering robust feature representation for open environments [25]. While effective for addressing drift from new family emergence, this method requires managing numerous episodes to cover all families in the training set, significantly increasing complexity. Yang et al. [40] propose feature de-entanglement techniques aiming to reduce spurious correlations during training, preserving invariant information. However, these methods may overlook critical feature correlations, such as specific API calls or intent combinations (in Android apps) directly indicative of malicious behavior and only focus on target feature space. Similarly, feature stability metrics for linear classifiers offer insights for drift robustness but have limited applicability to non-linear models and complex feature interactions [2].

These prior methods seek to enhance invariant feature information by mitigating instabilities, which aligns with our approach. However, due to the diverse evolution and complexity of malware, pinpointing the precise cause of drift remains challenging. Strategies that rely on assumptions, such as drift

<sup>2</sup>We will open source the dataset metadata and code repository to foster reproducibility studies.

being driven by new malware families, are limited. Instead, recognizing that distribution drift inevitably occurs over time motivates our exploration of temporally invariant information.

## 2.2 Invariant Learning

Assume that the training data  $\mathcal{D}_{tr}$  is collected from multiple environments  $e \in \mathcal{E}$ , i.e.,  $\mathcal{D}_{tr} = \{\mathcal{D}_{tr}^e\}_{e \in \mathcal{E}}$ . Let the input space be  $x \in \mathcal{X}$  and the target space be  $y \in \mathcal{Y}$ , and for the sample observations from each environment denoted  $x, y \sim p(x, y|e)$ , the samples within the environments obey an independent and identical distribution. Suppose a classification model  $f$ , denoted as a composite function  $f = c \circ \phi$ , where  $\phi : \mathcal{X} \rightarrow \mathcal{H}$  denotes a feature encoder that maps the input samples into a feature representation space  $\mathcal{H}$ , and  $\phi(x) \in \mathcal{H}$  is the “representation” of sample  $x$ . The  $c : \mathcal{H} \rightarrow \mathcal{Y}$  denotes a classifier that maps the feature representation to the logits space of  $\mathcal{Y}$ .

### 2.2.1 Learning Invariant Representation

In test environments where distribution drift exists, the test data  $\mathcal{D}_{te}$  may come from a distribution  $p(x, y|e_{te})$  that does not appear in the training set, i.e.  $e_{te} \notin \mathcal{E}$ . Robustness to drift yields lower error rates on unknown test data distributions.

Invariant learning enhances the generalization ability of a model to unknown distributions by learning label distributions that are invariant across training environments. Its goal is to develop a classifier  $c(\cdot)$  that satisfies the environmental invariance constraint (EIC) [13]:

$$\mathbb{E}[y | \phi(x), e] = \mathbb{E}[y | \phi(x), e'], \quad \forall e, e' \in \mathcal{E}, \quad (1)$$

where  $e$  and  $e'$  denote different environments to which the samples belong. This constraint is integrated into the training objective through a penalty term. Thus, the goal can be formalized as:

$$\min_f \sum_{e \in \mathcal{E}} R_{erm}^e(f) + \lambda \cdot \text{penalty}(\{S^e(f)\}_{e \in \mathcal{E}}), \quad (2)$$

where  $R_{erm}^e(f) = \mathbb{E}_{p(x, y|e)}[\ell(f(x), y)]$  represents the expected loss on environment  $e$ . Empirical risk minimization (ERM) is to minimize this expected loss within each environment.  $S^e(f)$  is some statistic of the model in  $e$  (see next), and the penalty is to constrain the change in this statistic to control the degree of deviation from the EIC. Optimizing this objective prevents mapping all  $x$  to the same value to satisfy environmental invariance, as it encourages the predictive utility of  $\phi$  by minimizing empirical risk loss. In addition, the form of the penalty term is variable to achieve constraints for different objectives. Krueger et al. [20] proposed V-Rex such that  $S^e(f) = R_{erm}^e(f)$ , to minimize the variance of  $S^e(f)$  in different environments. In CLOvE [33], the penalty is defined as the sum of the calibration errors of the model in each environment. One widely used scheme is Invariant Risk Minimization (IRM) and its practical variant IRMv1 proposed by Arjovsky et al. [3]. The

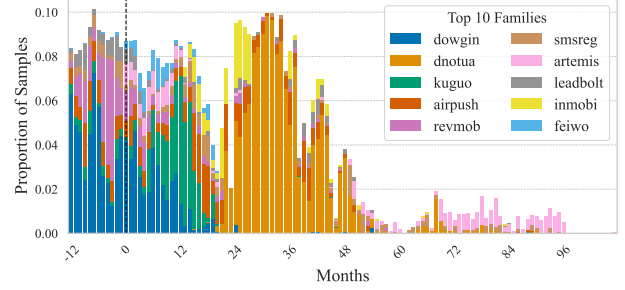


Figure 1: The top-10 families’ proportions vary over time; zero marks the test start, negatives indicate training.

penalty term is the sum of  $S^e(f) = \|\nabla_w R_{erm}^e(w \circ \phi)\|^2$ .  $w$  is a constant scalar multiplier of 1.0 for each output dimension, forcing the same classifier to be optimal in all environments.

### 2.2.2 Split Environments for Invariant Learning

Invariant learning relies on segmenting environments to highlight differences across them [8]. Early methods assumed prior knowledge of environment labels, which is often unavailable in practice [1, 14, 22, 30]. Recent approaches focus on invariant learning without predefined labels. Creager et al. [13] proposes estimating environment labels via prior clustering before applying invariant learning (EIIL), while others explore segmentation strategies such as natural clustering using dataset-provided labels or unsupervised clustering [32]. Experiments show natural clustering outperforms unsupervised methods. Regardless of the approach, effective segmentation requires environments to expose unstable information that can be ignored during invariant learning [8].

## 3 Motivation

Learning-based malware detectors deliver outstanding performance in identifying potential threats; however, maintaining consistent performance under drift scenarios remains challenging. Figure 1 supports this claim, depicting the monthly proportion changes of the top-10 dominant families in our dataset (Section 5.1.1) across the training and testing phases. Notably, some families that dominate during training, such as Dowgin, gradually disappear in the testing phase, while new families, like Artemis, emerge. This dynamic evolution poses challenges for malware detectors’ generalization across families. Even for families like Airpush, present in both phases, its feature distribution is also influenced by multiple factors including temporal fluctuations in proportions and API changes.

### 3.1 Threat Model

Malware natural drift refers to the gradual evolution of malware distributions over time, driven by the emergence of new

families and modifications to existing ones. Without knowledge of detection methods, attackers can alter malware features, causing distribution shifts that undermine the long-term effectiveness of detection systems.

Our threat model focuses on natural drift, which differs from adversarial attacks that rely on knowledge of the detection scheme to identify optimal perturbations for evading models [28]. We find that even natural drift disrupts the adaptation capabilities of traditional methods, hindering their ability to generalize to new distributions. Therefore, in this work, we address the long-term challenges posed by malware natural drift by enhancing the robustness of detection systems against malware evolution. We consider adversarial drift to be out of scope for this paper and plan to explore it in future work.

### 3.2 Invariance in Malware Evolution

The challenges highlighted in Section 3.1 motivate the search for characteristics from training set which can be generalized to test samples. Indeed, definitions of malware families and types have inspired the exploration of such invariance by categorizing malware according to code structure, behavioural patterns and malicious intent. While specific implementations may vary due to evolutionary or obfuscation techniques, members of the same family typically exhibit behavioral patterns consistent with their overall goals. Furthermore, malware types similarly represent a wide range of operational intentions that remain stable across families. These internal consistencies form the basis of invariance, which we categorize as inter-family invariance and intra-family invariance: **Intra-family invariance:** Variants within a malware family maintain consistent operational behaviors and attack strategies, despite differences in implementation. **Inter-family invariance:** Common malicious patterns observed across malware families, such as resource abuse or evasion techniques.

To illustrate invariant malicious behaviors in drift scenarios, we select APKs from Androzoo<sup>3</sup> and decompile them using JADX<sup>4</sup> to obtain .java files. Our analysis focuses on core malicious behaviors in the source code. For intra-family invariance, we use versions of the Airpush family, known for intrusive ad delivery, from different periods. For inter-family invariance, we examine the Hiddad family, which shares aggressive ad delivery and tracking tactics but uses broader permissions, increasing privacy risks. Figure.2 shows code snippets with colored boxes highlighting invariant behaviors across samples. While Airpush uses asynchronous task requests, Hiddad relies on background services and scheduled tasks to evade detection.

Figure 2(a)<sup>5</sup> and (b)<sup>6</sup> show core code from this family in 2014 and later years, respectively. The 2014 version

uses `NotifyService` and `TimerTask` to notify users every 24 hours, maintaining ad exposure. The later version, adapting to Android 8.0’s restrictions, triggers `NotifyService` via `BroadcastReceiver` with `WAKE_LOCK` to sustain background activity. In Drebin’s [4] feature space, these invariant behaviors are captured through features like `android_app_NotificationManager;notify`, `permission_READ_PHONE_STATE` and so on. Both implementations also use `URLConnection` for remote communication, asynchronously downloading ads and tracking user activity, and sharing Drebin features such as `java/net/URLConnection` and `android_permission_INTERNET`.

Similarly, Figure. 2(c)<sup>7</sup> shows a real sample from the Hiddad family, which uses HTTP connections for ad delivery, along with `AnalyticsServer` and `WAKE_LOCK` for continuous background services. Permissions like `android_permission_WAKE_LOCK` and API calls such as `getService` reflect shared, cross-family invariant behaviors, whose learning would enhance model detection across variants.

Capturing the core malicious behaviors of Airpush aids in detecting both new Airpush variants and the Hiddad family, as they share similar malicious intents. These stable behaviors form consistent indicators in the feature space. However, detectors with high validation performance often fail to adapt to such variants, underscoring the need to investigate root causes and develop a drift-robust malware detector.

*Take Away: The feature space of training samples contains invariance within and among malware families to be learned.*

### 3.3 Failure of Learning Invariance

Let  $f_r \in \mathcal{R}$  be a sample in the data space with label  $y \in \mathcal{Y} = \{0, 1\}$ , where 0 represents benign software and 1 represents malware. The input feature vector  $x \in \mathcal{X}$  includes features  $\mathcal{F}$  extracted from  $f_r$  according to predefined rules. The goal of learning-based malware detection is to train a model  $\mathcal{M}$  based on  $\mathcal{F}$ , mapping these features into a latent space  $\mathcal{H}$  and passing them to a classifier for prediction. The process is formally described as follows:

$$\arg \min_{\theta} R_{erm}(\mathcal{F}), \quad (3)$$

where  $\theta$  is the model parameter to be optimized and  $R_{erm}(\mathcal{F})$  represents the expected loss based on features space  $\mathcal{F}$ , defined as:

$$R_{erm}(\mathcal{F}) = \mathbb{E}[\ell(\hat{y}, y)]. \quad (4)$$

$\ell$  is a loss function. By minimizing the loss function,  $\mathcal{M}$  achieves the lowest overall malware detection error.

<sup>3</sup><https://androzoo.uni.lu>

<sup>4</sup><https://github.com/skylot/jadx>

<sup>5</sup>MD5: 17950748f9d37bed2f660daa7a6e7439

<sup>6</sup>MD5: ccc833ad11c7c648d1ba4538fe5c0445

<sup>7</sup>MD5: 84573e568185e25c1916f8fc575a5222

Airpush version 1	Airpush version 2	Hiddad
<pre> AsyncTask&lt;Void, Void, Void&gt; downloader = new AsyncTask&lt;Void, Void, Void&gt;() { @Override protected Void doInBackground(Void... params) { URL u = new URL(thisUrl); urlConnection = (URLConnection) u.openConnection(); urlConnection.setInstanceFollowRedirects(true); InputStream is = urlConnection.getInputStream(); @Override protected void onPostExecute(Void result) { completion.run();}}; UrlImageViewHelper.executeTask(downloader); this.timer.schedule(new TimerTask() { @Override public void run() { NotificationManager nm = (NotificationManager) nm.notify(NotificationService.this.notificationID, mBuilder.build()); ... }, 0L, 86400000L); (a) </pre>	<pre> public final void run() { URLConnection httpURLConnection; httpURLConnection = (URLConnection) new URL(q.(a[b[5], b[2]L; b[5]).intern()).openConnection(); ... InputStream inputStream = httpURLConnection.getInputStream(); BufferedReader bufferedReader = new BufferedReader(new InputStreamReader(inputStream)); ... thread.start(); AdView.this.handler.post(new AnonymousClass1());} public class MyReceiver extends BroadcastReceiver { Intent myIntent = new Intent(context, NotifyService.class); context.startService(myIntent); if (wakeLock == null) { PowerManager powerManager = (PowerManager) context.getSystemService(Context.POWER_SERVICE); wakeLock = powerManager.newWakeLock(PowerManager.PARTIAL_WAKE_LOCK, " MyApp:AnalyticsWakeLock"); wakeLock.setReferenceCounted(false); } wakeLock.acquire(1000L); (b) </pre>	<pre> public class h { public static Bitmap a(String str) {... URLConnection httpURLConnection = (HttpURLConnection) new URL(str).openConnection(); URLConnection connect(); Bitmap decodeStream = BitmapFactory.decodeStream(new a(httpURLConnection.getInputStream()); httpURLConnection.disconnect()); return decodeStream; } public final class AnalyticsReceiver extends BroadcastReceiver { ... public void onReceive(Context context, Intent intent) { if ("com.google.android.gms.analytics.ANALYTICS_DISPATCH" equals(intent.getAction())) { context.startService(new Intent(context, AnalyticsService.class)); if (wakeLock == null) { PowerManager powerManager = (PowerManager) context.getSystemService(Context.POWER_SERVICE); wakeLock = powerManager.newWakeLock(PowerManager.PARTIAL_WAKE_LOCK, " AnalyticsWakeLock"); wakeLock.setReferenceCounted(false); } wakeLock.acquire(1000L); (c) </pre>

① Get ad data from a specific URL ② Asynchronous execution to avoid user interruption ③ Push ads continuously through the background service

Figure 2: (a), (b), and (c) show real code snippets from an early Airpush version, a later Airpush version, and the Hiddad adware family. Airpush’s core behavior includes: (1) getting ad data from a specific URL, (2) asynchronous execution to avoid user interruption, and (3) pushing ads continuously through the background service. (a) and (b) demonstrate that both Airpush versions share invariant behaviors, with similar API calls and permissions despite implementation differences. Hiddad, while skipping step (2) for simpler ad display, shares steps (1) and (3) with Airpush, especially the newer version.

### 3.3.1 Stability and Discriminability of Features

To investigate the drift robustness in malware evolution from the feature perspective, we define two key feature properties: stability and discriminability. Stability refers to a feature’s ability to maintain consistent relevance across distributions, while discriminability reflects a feature’s capacity to effectively distinguish categories. To avoid model-induced biases, we propose a modelless formal definition applicable to diverse architectures.

Let  $f_j$  represent the  $j$ -th feature in the feature set  $\mathcal{F}$ , and  $S$  denote the set of all samples. To capture the behavior of feature  $f_j$  under different conditions, we compute its active ratio over a subset  $S' \subseteq S$ , representing how frequently or to what extent the feature is “active” within that subset. Specifically, for a binary feature space, feature  $f_j$  takes values 0 or 1 (indicating the absence or presence of the feature, respectively), the active ratio of  $f_j$  in the subset  $S'$  is defined as the proportion of samples where  $f_j$  is present, which is defined as Eq. 5:

$$r(f_j, S') = \frac{1}{|S'|} \sum_{s \in S'} f_j(s). \quad (5)$$

The ratio measures how frequently the feature is activated within the subset  $S'$  relative to the total number of samples in the subset. At this point, we can define the stability and discriminability of features.

**Definition 1. Stable Feature:** A feature  $f_j$  is defined as stable if, for any sufficiently large subset of samples  $S' \subseteq S$ , the active ratio  $r(f_j, S')$  remains within an  $\epsilon$ -bound of the overall active ratio  $r(f_j, S)$  across the entire sample set, regardless of variations in sample size or composition. Formally,  $f_j$  is

stable if:

$$\forall S' \subseteq S, |S'| \geq n_0, \quad |r(f_j, S') - r(f_j, S)| \leq \epsilon, \quad (6)$$

where  $\epsilon > 0$  is a small constant, and  $n_0$  represents a minimum threshold for the size of  $S'$  to ensure the stability condition holds.

When we consider discriminability, there is a need to focus on the category to which the sample belongs. Thus, let  $C = \{C_1, C_2, \dots, C_k\}$  be a set of  $k$  classes, and  $S_k \subseteq S$  be the subset of samples belonging to class  $C_k$ . The active ratio of feature  $f_j$  in class  $C_k$  is given by:

$$r(f_j, S_k) = \frac{1}{|S_k|} \sum_{s \in S_k} f_j(s). \quad (7)$$

**Definition 2. Discriminative Feature:** A feature  $f_j$  is discriminative if its active ratio differs significantly between at least two classes,  $C_p$  and  $C_q$ . Specifically, there exists a threshold  $\delta > 0$  such that:

$$\exists C_p, C_q \in C, p \neq q, \quad |r(f_j, S_p) - r(f_j, S_q)| \geq \delta. \quad (8)$$

Furthermore, the discriminative nature of the feature should be independent of the relative class sizes, meaning that the difference in activation should remain consistent despite variations in the proportion of samples in different classes. Mathematically, for any subset  $\tilde{S}_p \subseteq S_p$  and  $\tilde{S}_q \subseteq S_q$ , where  $|\tilde{S}_p| \neq |S_p|$  or  $|\tilde{S}_q| \neq |S_q|$ , the discriminative property still holds:

$$|r(f_j, \tilde{S}_p) - r(f_j, \tilde{S}_q)| \geq \delta. \quad (9)$$

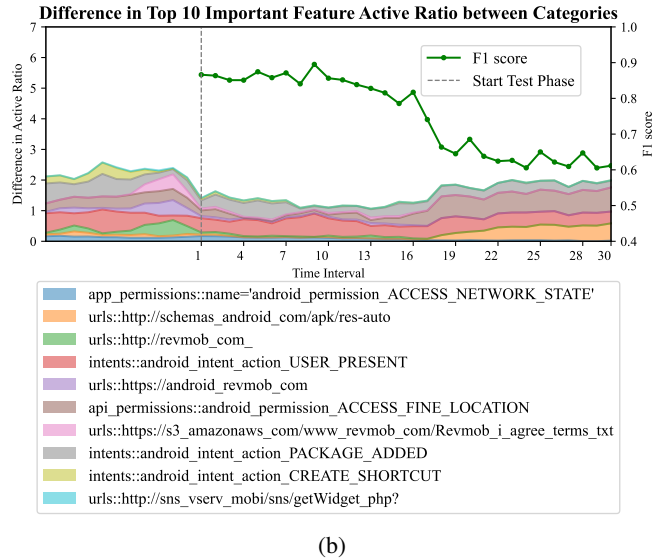
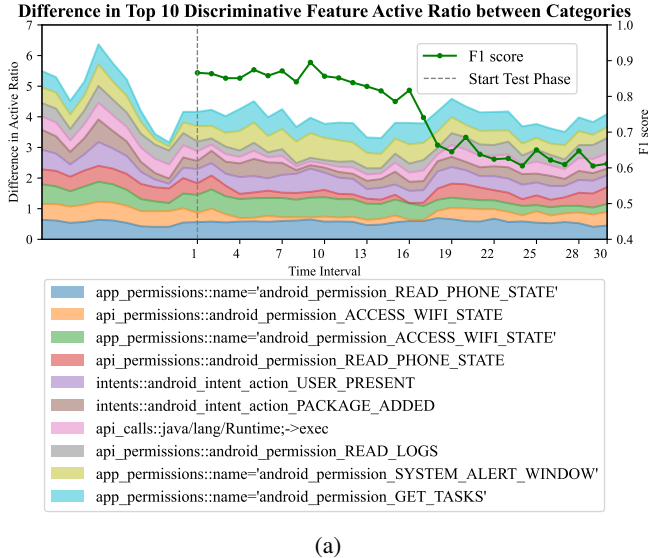


Figure 3: (a) and (b) illustrate changes in the discriminability of the top 10 discriminative training features and the top 10 important testing features, respectively. “Discriminability” is defined as the absolute difference in active ratios between benign and malicious samples. The grey dotted line indicates the start of the testing phase, with preceding values representing each feature’s discriminability across months in the training set.

### 3.3.2 Failure Due to Learning Unstable Discriminative Features

The malware detector’s strong performance within the same period indicates effective learning of discriminative features to separate benign software from malware. However, performance degradation over time stems from the model’s inability to capture stable discriminative features from the training set. To illustrate this, we randomly sample 110,723 benign and 20,790 malware applications from the Androzoo<sup>8</sup> platform (2014–2021). Applications are sorted by observation date, with 2014 samples used for training and the remainder divided into 30 test intervals. We extract Drebin [4] features, covering nine behavioral categories such as hardware components, permissions, and restrict API calls, and select the top 10 discriminative features based on active ratio differences to track over time. The model configuration follows DeepDrebin [17], a three-layer fully connected neural network with 200 neurons per layer. We evaluate performance in each interval using macro-F1 scores. As shown in Figure 3, although the top 10 discriminative features maintain stable active ratios, the detector’s performance consistently declines. We further examine feature importance over time using Integrated Gradients (IG) with added binary noise, averaging results across five runs to ensure robustness, as recommended by Warnecke et al. [34].

Figure 3 compares the active ratios of top discriminative (a) and important features (b). While stable discriminative features persist, ERM-based detectors often rely on unsta-

ble features with fluctuating effectiveness, leading to poor generalization under drift.

We observe that highly discriminative features, such as `api_calls::java/lang/Runtime;->exec` and `GET_TASKS`, are often linked to high-permission operations and potential malicious activity. These features, rarely seen in legitimate applications, reflect malware invariance, where core malicious intents persist despite evolving implementations.

**Take Away:** *There are stable and highly discriminative features representing invariance in the training samples, yet current malware detectors fail to learn these features leading to decaying models’ performance.*

### 3.4 Create Model to Learn Invariance

This discussion emphasizes the importance of learning stable, discriminative features for drift-robust malware detection. ERM captures both stable and unstable information correlated with the target variable [10], often relying on unstable features when they are highly correlated. The key challenge is to isolate and enhance stable features, aligning with the principles of invariant learning in Section 2.2.

Invariant learning methods face challenges, as their success depends on effective environment segmentation to reveal unstable information [23, 30]. In malware detection, identifying variants that trigger distribution shifts is uncertain. High-quality representations from the encoder are also essential for invariant predictors [38], yet Figure 3 shows that even

<sup>8</sup><https://androzoo.uni.lu>

during training, features fail to distinguish goodware from malware or capture malware’s execution intent, relying on ambiguous cues.

To this end, we propose a temporal-aware environment segmentation method to reveal the instability of malware distribution drifts. In each environment, the ERM hypothesis guides the association with the target variable, and an encoder shared across environments attempts to learn all stable and unstable representations, after which it enhances the detector’s generalization by minimizing the invariant risk to filter unstable elements.

*Take Away: Invariant learning helps to learn temporal stable features, but it is necessary to ensure that the training set can expose unstable information and the encoder can learn good and diverse representations.*

## 4 Methodology

### 4.1 Preliminary

#### 4.1.1 Notations

We use uppercase and lowercase letters to denote matrices and vectors, respectively;  $|\mathcal{D}|$  represents the total number of elements in set  $\mathcal{D}$ .

#### 4.1.2 Problem setting

In Android malware detection, samples  $x \in \mathbb{R}^d$  are divided into two parts: the labeled training data  $\mathcal{D}_{tr} = (x_i^{tr}, y_i^{tr})_{i=1}^{|\mathcal{D}_{tr}|}$ , where  $y_i^{tr} \in \{0, 1\}$  represents the labels for benign and malicious applications, and the unlabeled test data  $\mathcal{D}_{ts}$ . Training data  $\mathcal{T}_{tr}$  comes from a specific period  $\mathcal{T}_{tr}$ , with each sample  $x_i^{tr}$  contains its corresponding observation timestamp  $t_i^{tr}$ . Test data  $\mathcal{D}_{ts}$  comprises future samples  $t_i^{ts} > \mathcal{T}_{tr}$  that appear progressively over time. We assume that the training and test data share the same label space and have unknown semantic similarities. The model is defined as  $\mathcal{M} = c \circ \phi$ , where  $c$  denotes the classifier and  $\phi$  is the feature encoder. This work aims to enhance the encoder in capturing invariant semantic features from training data that generalize to unseen test data.

### 4.2 Overall Architecture

Section 3.3.2 highlights the need for learning temporally stable and discriminative features to improve robustness against distribution drift. We propose a temporal invariant training method, adaptable to any malware detector, which enhances robustness by extracting rich features and suppressing unstable factors through invariant risk minimization. The method comprises two components: **Multi-Proxy Contrastive Learning (MPC)**: representation diversity for benign and malware samples with dynamic proxies, encoding complex multi-family malware semantics into compact,

discriminative embeddings. **Invariant Gradient Alignment (IGA)**: This component applies invariant risk minimization (IRM) to align gradients across environments, enabling the encoder to learn unified representations over time.

Figure 4 illustrates the overall framework of the proposed method, where Android applications are divided into non-overlapping environments based on their observation dates. The invariant training process includes two stages:

- Discriminative Information Amplification Stage: MPC is applied within each environment to minimize empirical risk, enabling the encoder to integrate discriminative features from each environment.
- Unstable Information Compression Stage: Building on the model trained in the first stage, MPC aligns features across environments, followed by IGA fine-tuning with IRM to suppress unstable information.

### 4.3 Training Environments Segmentation

Segmenting the training environment requires exposing unstable information. Malware distribution drift arises from multiple factors, such as application market demands or Android version updates. Dividing the training environment based on application observation dates effectively captures this mix of unknown causes. For a dataset with timestamps from  $T_{\min}$  to  $T_{\max}$ , and a chosen time granularity  $\Delta$ , samples are divided into  $t$  time windows, each representing an environment  $e \in \mathcal{E}$ , where  $|\mathcal{E}| = t$ . The resulting training set is an ordered multiset,  $\mathcal{D} = \{D_1, D_2, \dots, D_t\}$ , with each environment  $D_t$  containing  $|D_t|$  samples. A sample  $x_i$  with timestamp  $t_i$  is assigned to an environment using:

$$\mathcal{E}(x_i) = \left\lfloor \frac{t_i - T_{\min}}{\Delta} \right\rfloor. \quad (10)$$

As the environment index increases, timestamps approach the present. Time granularity impacts representation learning, balancing detailed distribution patterns against sample sufficiency. Finer granularity risks sparse samples, while coarser granularity may obscure shifts. Achieving balance requires careful consideration of label distribution to avoid misaligned representations. Section 5.6 explores the effects of granularity choices.

### 4.4 Multi-Proxy Contrastive Learning

Malware families have distinct distributions and imbalanced sample sizes, complicating malware category modeling in the embedding space. Benign samples may also display complex feature distributions due to factors like geographic location or user behavior. Treating all relationships within a single family equally can exacerbate imbalances, while overly homogenizing samples overlook valuable information. Thus, effective

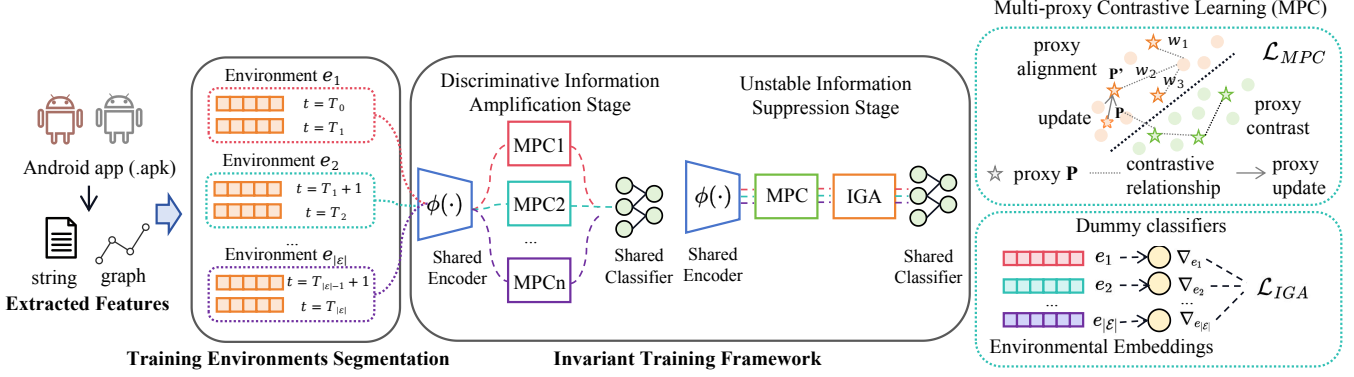


Figure 4: The proposed invariant training framework and its core components

discrimination requires balancing the complex pairwise relationships within each category to ensure high-quality representations that capture diversity. To address this, we introduce a multi-proxy contrastive learning method, where each proxy represents a subset of samples with similar behaviors or structures in one category, and is dynamically updated to trade-off between consistency and diversity of representations.

For a given batch of samples  $\mathbf{X}_c \in \mathbb{R}^{|\mathcal{B}_c| \times d}$  from category  $c$ , where  $|\mathcal{B}_c|$  is the batch size and  $d$  is the feature dimension, we randomly initialize  $K$  proxies for both benign and malicious categories. Each sample is then assigned to relevant proxies. In this multi-proxy setup, avoiding dominance by any single proxy helps mitigate noise. Inspired by the Sinkhorn [15] algorithm, we compute a probability matrix  $\mathbf{W}_c$  for proxies within category  $c$ , assigning a weight  $w_{ij}$  to proxy  $j$  for each sample  $x_i$  as follows:

$$w_{ij}^{(c)} = \frac{u_i \cdot \exp\left(\text{sim}(\mathbf{x}_i, \mathbf{P}_c^{(j)})/\epsilon\right) \cdot v_j}{\sum_{i=1}^{|\mathcal{B}_c|} \sum_{j=1}^K u_i \cdot \exp\left(\text{sim}(\mathbf{x}_i, \mathbf{P}_c^{(j)})/\epsilon\right) \cdot v_j}, \quad (11)$$

where  $\epsilon$  is a temperature parameter controlling the smoothness of the assignment.  $\text{sim}(\mathbf{x}_i, \mathbf{P}_c^{(j)})$  represents the dot-product similarity between the sample and the proxy.  $u_i$  and  $v_j$  are auxiliary normalization factors to ensure that all assigned weights satisfy a doubly-normalized constraint, adjusted iteratively through row and column scaling.

To reduce the complexity, the top- $N$  proxies with larger weights are selected here to participate in the computation of the proxy loss. Thus, for the sample over the selected proxies, the proxy alignment loss is denoted as:

$$\mathcal{L}_{pal} = -\frac{1}{|\mathcal{B}_c|} \sum_{c=1}^C \sum_{i=1}^{|\mathcal{B}_c|} \left( \sum_{j=1}^N \mathbf{W}_c^{(i,j)} \cdot \log(p_{ij}^c) \right), \quad (12)$$

where  $p_{ij}^c$  is the softmax probability calculation for sample  $i$  and proxy  $j$  within each class  $c$ , represent as follow:

$$p_{ij}^c = \frac{\exp\left(\text{sim}(\mathbf{x}_i, \mathbf{P}_c^{(j)})/\tau\right)}{\sum_{k=1}^N \exp\left(\text{sim}(\mathbf{x}_i, \mathbf{P}_c^{(k)})/\tau\right)}, \quad (13)$$

where a temperature parameter  $\tau$  is applied to scale the similarities.

The distribution of proxies determines the diversity and compactness of the embedding. To ensure stable and meaningful similarity calculations, all proxies are normalized to the unit hypersphere. We make the inter-class proxies far away and the intra-class proxies close together, and here we propose the agent contrast loss as shown in Eq. 14. To distinguish proxy-to-proxy similarities from sample-proxy similarities, here we define the former similarity as  $\text{sim}_p(\mathbf{P}_c^{(i)}, \mathbf{P}_c^{(j)})$ .

$$\mathcal{L}_{pcl} = -\frac{1}{K} \sum_{c=1}^C \sum_{i=1}^K \log(\tilde{p}_{ij}^c) + \frac{1}{C(C-1)} \sum_{c=1}^C \sum_{c_1=1, c_2 \neq c_1}^C \max_{i,j} \mathbf{P}_{c_1}^{(i)\top} \mathbf{P}_{c_2}^{(j)}. \quad (14)$$

Similarly,  $\tilde{p}_{ij}^c$  denotes the computation of softmax probability between proxy  $i$  and proxy  $j$  in category  $c$ , i.e:

$$\tilde{p}_{ij}^c = \frac{\exp\left(\text{sim}_p\left(\mathbf{P}_c^{(i)}, \mathbf{P}_c^{(j)}\right)/\tau\right)}{\sum_{k=1, k \neq i}^K \exp\left(\text{sim}_p\left(\mathbf{P}_c^{(i)}, \mathbf{P}_c^{(k)}\right)/\tau\right)}. \quad (15)$$

During training, category proxies are updated using a momentum strategy to adapt to evolving application distributions. Updates combine the weighted sum of the previous proxy matrix and the samples associated with each proxy. The updated proxies  $\mathbf{P}'_c$  of class  $c$  are computed as follows:

$$\mathbf{P}'_c = \gamma \mathbf{P}_c + (1 - \gamma) \mathbf{W}_c^T \mathbf{X}_c, \quad (16)$$

where  $\gamma$  is the momentum coefficient controlling the update rate. Therefore, we can obtain the multi-proxy contrastive loss as the training objective in this module, which can be formalized as:

$$\mathcal{L}_{MPC} = \mathcal{L}_{pal} + \lambda \cdot \mathcal{L}_{pcl}, \quad (17)$$

where  $\lambda$  balance the weight of these two loss functions.



## 4.5 Invariant Gradient Alignment

Section 3.4 highlights the prerequisites for learning invariant features: environment segmentation to expose unstable information and rich feature representations. Building on the definition of Invariant Risk Minimization (IRM) in Section 2.2, our goal is to guide encoders to focus on the stable aspects of these representations. To achieve this, the encoder must ensure that representations of the same class across different environments produce similar classifier gradients. We introduce an invariant gradient alignment module based on IRMv1 [3] to enhance the model’s focus on invariant features. The objective function is shown in Eq. 18.

$$\mathcal{L}_{IGA} = \frac{1}{|\mathcal{E}|} \sum_{e \in \mathcal{E}} \|\nabla_{s_e|s_e=1.0} R^e(s_e \circ \phi)\|^2. \quad (18)$$

Here,  $s_e$  acts as a scalar, serving the role of a dummy classifier, set to 1.0 and updates through gradient backpropagation.  $\mathcal{L}_{grad}$  evaluates how adjusting  $s_e$  minimizes the empirical risk in environment  $e$ .  $R^e(s_e \circ \phi)$  is represented as Eq. 19:

$$R^e(s_e \circ \phi) = \mathbb{E}^e[\mathcal{L}_{CLS}(s_e(\phi(x)), y)], \quad (19)$$

where  $\mathcal{L}_{CLS}$  denotes the classification loss function used in the current environment, such as binary cross-entropy for malware detection. This loss is computed following standard ERM training. The term  $\phi(x)$  represents the output of the shared encoder for samples  $x, y \sim p(x, y|e)$  from environment  $e$ . The gradient penalty term encourages uniform feature representation by aligning gradients of classifiers across environments, thereby promoting consistent model performance.

## 4.6 Invariant Training Framework

Gradient adjustment for invariant learning classifiers relies heavily on the encoder’s ability to learn rich representations [44]. Starting from random initialization often leads to suboptimal convergence. To overcome this, we propose a two-stage training strategy to first capture diverse features before applying invariant learning.

### 4.6.1 Discriminative Information Amplification

In the first stage, ERM training is conducted independently for each environment to initialize the encoder. The multi-proxy contrastive learning module is then applied to each environment to maximize the exploitation of discriminative features. The optimization objective is defined in Eq. 20:

$$\mathcal{L}_{ERM} = \frac{1}{|\mathcal{E}|} \sum_{e \in \mathcal{E}} (\mathcal{L}_{CLS}^e + \alpha \cdot \mathcal{L}_{MPC}^e), \quad (20)$$

where  $\mathcal{L}_{CLS}^e$  and  $\mathcal{L}_{MPC}^e$  denote the classification loss and multi-proxy contrastive loss for environment  $e$ , respectively. Jointly minimizing the empirical risk across all environments equips the encoder with diverse feature representations, forming a robust foundation for invariant training.

### 4.6.2 Unstable Information Suppression

To mitigate overfitting to environment-specific features from the earlier stage, we reset the optimizer’s parameters before the second training phase. This reset allows the model to refocus on the objectives of invariant learning. In this phase, we first apply a multi-proxy contrastive loss across all samples to enhance class representation learning. Next, invariant gradient alignment is used to harmonize classification gradients across environments. The updated optimization objective is defined in Eq. 21:

$$\mathcal{L}_{IRM} = \mathcal{L}_{CLS} + \alpha \cdot \mathcal{L}_{MPC} + \beta \cdot \mathcal{L}_{IGA}, \quad (21)$$

In training, the hyperparameters  $\alpha$  and  $\beta$  balance the contributions of each loss term. This two-stage approach enables the model to first capture a broad feature set, then refine it for cross-environment invariance, enhancing generalization under distribution shifts. The pseudo-code of the training process is shown in Appendix D.

## 5 Evaluation

This section evaluates the effectiveness of our proposed method in improving drift robustness for Android malware detectors across various feature spaces. We also analyze the contributions of each component in the invariant learning framework. The evaluation addresses the following research questions:

- RQ1.** Can our framework mitigate detector aging across different feature spaces?
- RQ2.** Can our framework stabilize detectors in different drift scenarios?
- RQ3.** Does our framework effectively learn invariant features of applications?

To ensure reliability, experiments were conducted using random seeds (1, 42, 2024), with results averaged. All experiments ran on an RTX A6000. The dataset and code will be released upon paper acceptance.

## 5.1 Evaluation Settings

### 5.1.1 Dataset

To evaluate the effectiveness of our approach in the context of long-term malware evolution, we select Android APKs from the Androzoo<sup>9</sup> platform and construct datasets based on the time when each software was discovered (i.e., when the sample was submitted to VirusTotal<sup>10</sup> for detection<sup>11</sup>)

<sup>9</sup><https://androzoo.uni.lu>

<sup>10</sup><https://www.virustotal.com>

<sup>11</sup>Due to the modifiable or randomly generated release time of Android applications, some timestamps (dex date) are unreliable.

Table 1: AUT(F1,12m) of the candidate detectors on future year samples before and after adding different baselines and our framework to different feature spaces. *w/o* denotes the unmodified original classifier; all classifiers are trained based on 2014 samples.  $\Delta$  denotes the performance percentage (%) between the proposed scheme and the base detector.

Test Years	Drebin [4]			DeepDrebin [17]				Malscan [35]			BERTroid [7]		
	w/o	T-stability [2]	Ours	w/o	APIGraph [45]	Guide [16] Retraining	Ours	w/o	Guide [16] Retraining	Ours	w/o	Guide [16] Retraining	Ours
2015	0.858	0.824	0.928	0.859	0.868	0.814	0.928	0.842	0.851	0.902	0.771	0.772	0.833
$\Delta$		$\downarrow$ 3.96	$\uparrow$ 8.16		$\uparrow$ 1.05	$\downarrow$ 5.24	$\uparrow$ 8.03		$\uparrow$ 1.07	$\uparrow$ 7.13		$\uparrow$ 0.01	$\uparrow$ 8.04
2016	0.811	0.782	0.877	0.813	0.818	0.749	0.877	0.799	0.795	0.850	0.744	0.743	0.789
$\Delta$		$\downarrow$ 3.58	$\uparrow$ 8.14		$\uparrow$ 0.06	$\downarrow$ 7.87	$\uparrow$ 7.87		$\downarrow$ 0.50	$\uparrow$ 6.38		$\downarrow$ 0.13	$\uparrow$ 6.05
2017	0.750	0.717	0.815	0.752	0.754	0.656	0.815	0.739	0.734	0.783	0.708	0.713	0.752
$\Delta$		$\downarrow$ 4.40	$\uparrow$ 8.67		$\uparrow$ 0.03	$\downarrow$ 12.77	$\uparrow$ 8.38		$\downarrow$ 0.68	$\uparrow$ 5.95		$\uparrow$ 0.71	$\uparrow$ 6.21
2018	0.724	0.718	0.794	0.726	0.726	0.623	0.794	0.713	0.708	0.755	0.686	0.694	0.726
$\Delta$		$\downarrow$ 0.83	$\uparrow$ 9.67		0.00	$\downarrow$ 14.19	$\uparrow$ 9.37		$\downarrow$ 0.70	$\uparrow$ 5.89		$\uparrow$ 1.74	$\uparrow$ 2.19
2019	0.700	0.726	0.769	0.713	0.713	0.575	0.769	0.700	0.694	0.741	0.660	0.670	0.701
$\Delta$		$\uparrow$ 3.71	$\uparrow$ 9.86		0.00	$\downarrow$ 19.35	$\uparrow$ 7.85		$\downarrow$ 0.86	$\uparrow$ 5.86		$\uparrow$ 2.42	$\uparrow$ 6.36
2020	0.665	0.723	0.732	0.700	0.696	0.527	0.732	0.687	0.681	0.726	0.630	0.641	0.674
$\Delta$		$\uparrow$ 8.72	$\uparrow$ 10.08		$\downarrow$ 0.57	$\downarrow$ 24.71	$\uparrow$ 4.57		$\downarrow$ 0.87	$\uparrow$ 5.68		$\uparrow$ 2.70	$\uparrow$ 7.14
2021	0.645	0.716	0.717	0.689	0.686	0.497	0.717	0.676	0.669	0.713	0.609	0.623	0.653
$\Delta$		$\uparrow$ 11.01	$\uparrow$ 11.16		$\downarrow$ 0.44	$\downarrow$ 27.87	$\uparrow$ 4.06		$\downarrow$ 1.04	$\uparrow$ 5.47		$\uparrow$ 3.28	$\uparrow$ 7.72
2022	0.616	0.687	0.688	0.661	0.658	0.450	0.688	0.643	0.635	0.680	0.583	0.597	0.627
$\Delta$		$\uparrow$ 11.53	$\uparrow$ 11.69		$\downarrow$ 0.45	$\downarrow$ 31.92	$\uparrow$ 4.84		$\downarrow$ 1.24	$\uparrow$ 5.75		$\uparrow$ 3.43	$\uparrow$ 8.06
2023	0.590	0.662	0.665	0.638	0.635	0.413	0.665	0.615	0.607	0.652	0.558	0.574	0.602
$\Delta$		$\uparrow$ 12.20	$\uparrow$ 12.71		$\downarrow$ 0.47	$\downarrow$ 34.64	$\uparrow$ 4.23		$\downarrow$ 1.30	$\uparrow$ 6.02		$\uparrow$ 2.87	$\uparrow$ 8.42

spanning the period from 2014 to 2023 dataset. A detailed description of the dataset can be found in the Appendix A. In subsequent experiments, the training set is samples from 2014 and the test set covers the remaining 9 years, where the training set is further divided into a proper training set (80%) and a validation set (20%).

### 5.1.2 Candidate Detectors

In Android malware detection, an APK file serves as input, containing the codebase (e.g., .dex files) and configuration files (e.g., manifest.xml), which offer behavioral insights such as API calls and permissions then organized as different formats. We select three representative feature spaces: Drebin [4] (vector-based), Malscan [35] (graph-based), and BERTroid [7] (string-based), each using distinct feature sources (details in Appendix B). For fair evaluation, we apply a two-layer linear classifier to each feature representation, with the final layer performing binary classification.

### 5.1.3 Baseline

To evaluate the robustness of our scheme across different feature spaces, we compare it with two non-linear baselines: (1) APIGraph [45], which enhances robustness using API-based features, and (2) Guided Retraining [16], which improves detector performance across multiple feature spaces. We also include T-stability [2], a feature stability method for linear classifiers in the Drebin feature space, to demonstrate the

advantages of our non-linear approach. Details on these baselines are provided in Appendix C.

### 5.1.4 Metrics

We evaluate different approaches using static and dynamic metrics. For static evaluation, the macro-F1 score is used to address the class imbalance in the Android dataset, offering a balanced assessment of precision and recall on a fixed-time test set. For dynamic evaluation, we employ the Area Under Time (AUT), a metric proposed by TESSERACT [27], which measures performance over time. AUT is calculated as:

$$\text{AUT}(m, N) = \frac{1}{N-1} \sum_{t=1}^{N-1} \left( \frac{m(x_{t+1}) + m(x_t)}{2} \right), \quad (22)$$

where  $m$  represents the performance metric, with the F1-score selected as its instance.  $m(x_t)$  denotes the performance metric at time  $t$ , and  $N$  is the number of monthly testing slots. AUT ranges from  $[0, 1]$ , with a perfect classifier achieving an AUT of 1 across all test windows.

## 5.2 Enhance Different Feature Space (RQ1)

This section evaluates the Temporal Invariant Learning Framework (TIF) for mitigating detector degradation across feature spaces. The classifier is trained on 2014 samples and tested monthly from 2015 to 2023, with annual results (AUT(F1, 12m)) summarized in Table 1. To optimize short-term performance, we use monthly partitioning, with segmentation

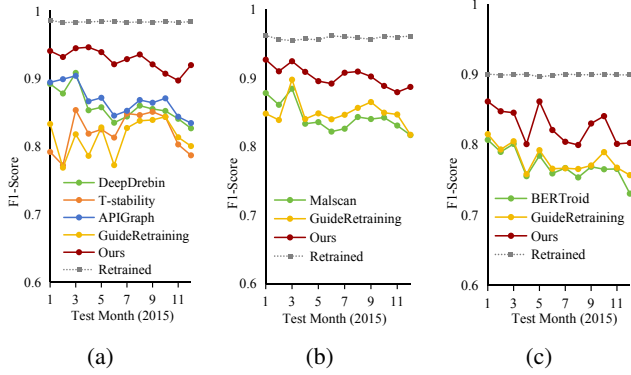


Figure 5: Monthly performance of DeepDrebin (a), Malscan (b), and BERTroid (c) during the first test year (2015), with models initially trained on 2014 data. *Retrained* denotes detectors updated monthly with labeled test samples.

granularity discussed in Section 5.6. Given that T-stability [2] is designed for the Drebin detector, we compare both the original Drebin [4] and its T-stability variant. APIGraph [45] supports Drebin and DeepDrebin but is incompatible with BERTroid [7] and Malscan [35], while GuideRetraining [16] applies to all detectors. We evaluate TIF against these baselines to assess absolute performance, noting that frequent switching between methods is impractical. Notably, TIF consistently outperforms others over the long term, even against the best yearly performances of alternative methods.

As drift increases over the test years, AUT declines for all methods, but TIF achieves up to an 8% improvement in the first year. This reflects real-world scenarios where detectors are retrained annually [45]. Figure 5 illustrates 2015 monthly performance, with a grey dashed line marking the upper performance bound. For each month  $n$ , training and validation sets include samples up to month  $n$ , simulating expert-labelled data for retraining. Without additional labels, TIF closely approaches this bound, demonstrating robust monthly gains. While AUT gains diminish over time, periodic retraining ensures manageable performance decline. T-stability performs poorly on early test samples but generalizes better to distant ones. Its design is tailored to a specific dataset, and changes in data composition affect its generalization. Moreover, it prioritizes feature stability over discriminability.

**Take Away:** TIF slows down the aging of detectors in each feature space and has significant performance gains in the years just after deployment.

### 5.3 Robustness in Different Drift Scenarios (RQ2)

This section evaluates how TIF aids malware detectors in learning stable representations under different drift scenarios.

Table 2: AUT(F1, 12m) of the closed-world drift and open-world test scenarios after adding different schemes in the DeepDrebin [17] detector. AG and GR represent baselines, APIGraph [45] and GuideRetraining [16], respectively

	Deepdrebin [17]							
	Closed world				Open world			
	w/o	AG	GR	Ours	w/o	AG	GR	Ours
1	0.911	0.920	0.906	0.949	0.903	0.905	0.871	0.918
2	0.880	0.891	0.861	0.927	0.860	0.863	0.788	0.879
3	0.855	0.865	0.808	0.902	0.817	0.822	0.714	0.839
4	0.811	0.821	0.727	0.861	0.764	0.771	0.657	0.788
5	0.777	0.789	0.663	0.827	0.727	0.735	0.602	0.752
6	0.758	0.770	0.627	0.805	0.705	0.713	0.541	0.730
7	0.742	0.754	0.598	0.788	0.689	0.698	0.497	0.715
8	0.733	0.645	0.573	0.778	0.678	0.687	0.443	0.705
9	0.728	0.739	0.552	0.771	0.671	0.679	0.692	0.697
10	0.714	0.723	0.529	0.756	0.658	0.665	0.415	0.682

We define two test scenarios based on drift factors: **Closed-world:** Test sets include only malware families from the training set (15,257 malware) and benign samples. **Open-world:** Test sets contain only families absent from the training set (2,920 malware) and benign samples. Due to uneven family distributions (Figure 1), we construct test sets by extracting normal samples corresponding to the time intervals covered by each test scenario and divided into 10 equal-length temporal segments for evaluation.

We evaluated the classification performance of DeepDrebin [17] detector with baselines and TIF in different scenarios, starting AUT(F1, 12m) calculations from the validation set. TIF improved AUT(F1, 12m) by 5.78% in closed-world and 3.17% in open-world settings. We computed the cosine similarity between malware representations in test intervals and the validation set to assess feature stability. Figure 6 shows the differences, with retrained detectors serving as ground truth. Results confirm that TIF consistently produces more stable feature representations in both scenarios, demonstrating robustness to drift.

**Take Away:** TIF generates stable feature representations for both evolved variants of existing families and new malware families.

### 5.4 Effective Invariant Feature Learning (RQ3)

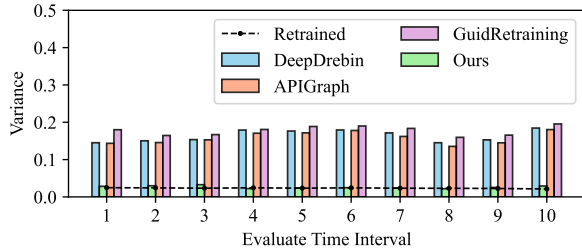
We evaluate the framework’s ability to learn invariant features. Section 3.3.2 shows that ERM models underperform by relying on unstable features. To quantify stable and discriminative feature learning, we define the Feature Contribution Score (FCS) for each feature  $f_j$  as follows:

$$FCS_j = |r(f_j, S_m) - r(f_j, S_b)| \cdot IS_j, \quad (23)$$

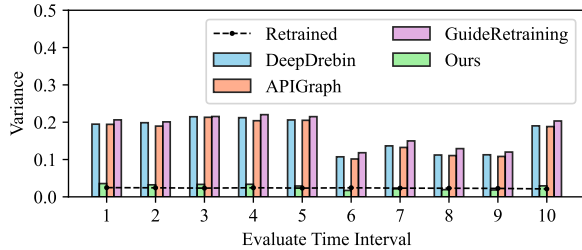
Table 3: The sum of feature contribution scores (FCS) for the comparison schemes during training and testing in both closed and open-world settings. AG and GR represent the baselines APIGraph [45] and GuideRetraining [16].

	DeepDrebin [17]							
	Closed world				Open world			
	w/o	AG	GR	Ours	w/o	AG	GR	Ours
Train	27.22	28.33	25.15	32.15	27.22	28.33	25.15	32.15
1	23.98	24.49	19.04	27.98	22.91	23.62	18.58	27.33
2	21.70	23.53	18.44	26.14	19.46	22.57	17.04	25.74
3	19.78	20.27	17.12	22.92	17.56	19.29	16.10	21.97
4	17.94	18.04	15.11	20.16	16.68	16.74	13.72	19.26
5	15.73	15.82	13.52	18.72	14.69	15.09	12.06	18.57
6	14.26	14.23	12.46	16.63	13.56	13.75	11.10	16.59
7	13.14	13.21	11.67	14.89	12.12	13.19	11.63	14.75
8	12.58	12.47	10.88	13.83	11.75	11.83	10.05	13.66
9	12.26	12.31	10.52	12.91	11.24	11.12	9.30	12.38
10	11.98	12.01	6.83	12.52	10.51	10.62	6.01	11.62

where  $r(f_j, S_m)$  and  $r(f_j, S_b)$  is the active ratio of feature  $f_j$  in malware and benign category respectively and  $IS_j$  is its importance score via integrated gradients (IG) with the malicious class as the target. For model  $\mathcal{M}$ , its discriminative ability is the sum of all FCS values, with higher scores indicating greater focus on discriminative features. We conduct interpretable Drebin [4] feature space experiments to visually assess this capability using closed and open-world settings, as outlined in Section 5.3. Results in Table 3 show that invariant training significantly raises FCS, guiding the model to more stable and discriminative features, thus enhancing robustness.



(a) Variance of representation similarity in closed-world setting



(b) Variance of representation similarity in open-world setting

Figure 6: The variance in malware feature representation similarity between detectors and the training set in closed-world (a) and open-world (b) scenarios. *Retrained* denotes detectors retrained at each time point with newly labeled samples.

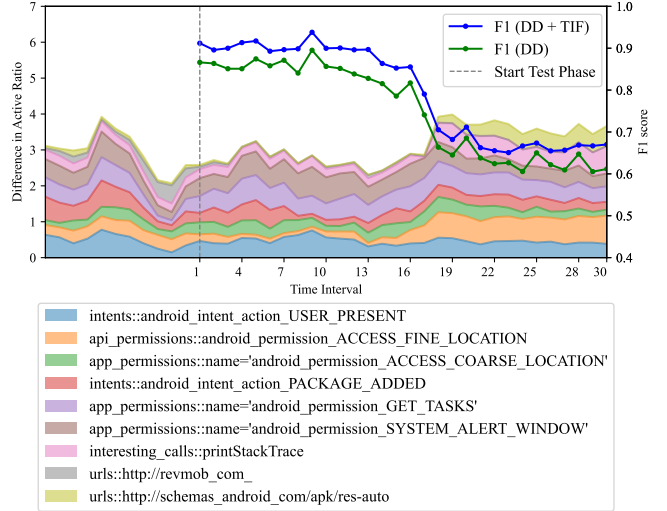


Figure 7: Discriminability for the Top-10 important features after invariant training. F1 Score (DD) represents DeepDrebin’s performance [17] trained as described in Section 3.3.2, while F1 Score (DD + TIF) reflects results after applying the TIF framework.

Table 4: AUR(F1, 12m) after adding different components on Deepdrebin detector. • means with; ◦ means without.

	DeepDrebin [17]				
	◦	•	•	◦	•
MPC1	◦	•	•	•	•
MPC2	◦	◦	•	◦	•
IGA	◦	◦	◦	•	•
2015	0.859	0.902	0.902	0.900	<u>0.928</u>
2016	0.813	0.847	0.854	0.856	<u>0.877</u>
2017	0.752	0.783	0.782	0.793	<u>0.815</u>
2018	0.726	0.760	0.750	0.771	<u>0.794</u>
2019	0.713	0.747	0.742	0.765	<u>0.769</u>
2020	0.700	0.719	0.731	0.743	<u>0.732</u>
2021	0.689	0.704	0.720	<u>0.731</u>	0.717
2022	0.661	0.667	0.686	<u>0.693</u>	0.688
2023	0.638	0.637	0.658	0.662	<u>0.665</u>

We also retrain the detector with TIF then analyze the top 10 important features and tracked their discriminability. Figure 7 shows improved F1 scores and greater stability in prioritized features. Permissions like GET\_TASK and ACCESS\_FINE\_LOCATION exhibit stronger correlations with malicious behavior, confirming that invariant training shifts focus to more robust features.

**Take Away:** TIF enables the detector to learn stable, discriminative features from the training set.

## 5.5 Ablation Study

This section evaluates the robustness of each component through an ablation study. Five configurations are tested: the

Table 5: AUT (F1, 12m) of the Deepdrebin [17] under different temporal environment segmentation methods.

Test Years	DeepDrebin [17]					
	w/o	monthly	quarterly	n=4	n=8	n=12
2015	0.859	<u>0.928</u>	0.915	0.914	0.902	0.905
2016	0.813	<u>0.879</u>	0.866	0.864	0.854	0.853
2017	0.752	<u>0.816</u>	0.801	0.800	0.783	0.799
2018	0.726	<u>0.794</u>	0.783	0.780	0.758	0.754
2019	0.713	0.769	<u>0.775</u>	0.762	0.745	0.741
2020	0.700	0.732	<u>0.764</u>	0.730	0.718	0.719
2021	0.689	0.717	<u>0.750</u>	0.709	0.701	0.705
2022	0.661	0.688	<u>0.717</u>	0.667	0.669	0.671
2023	0.638	0.665	<u>0.690</u>	0.634	0.643	0.645

base model, +MPC1, +MPC1 +MPC2, +MPC1 +IGA, and +MPC1 +IGA +MPC2, where MPC1/MPC2 represent multi-proxy contrastive learning in two training stage, and IGA denotes invariant gradient alignment which is only used in the second stage. Table 4 shows the AUT(F1, 12m) results for each setup with the Drebin detector.

MPC1 improves intra-environment representations, surpassing the baseline. Adding MPC2 and IGA enhances generalization by aligning gradients and capturing global features. The full configuration achieves the highest robustness by integrating stable and discriminative feature learning.

## 5.6 Environment Granularity Selection

Environment segmentation is crucial in invariant learning to expose uncertainty while ensuring sufficient samples per environment for effective training. We evaluate three segmentation granularities—monthly, quarterly, and equal-sized splits ( $n = 4, 8, 12$ ). Table 5 reports AUT(F1, 12m) scores across the test phase. Equal-sized splits increase label imbalance, hindering robust learning, while fine-grained splits improve feature discrimination but reduce per-batch samples, complicating cross-environment alignment. Therefore, when we need the model to be able to achieve short-term stability, monthly splitting is the superior choice.

## 6 Discussion

### 6.1 Influence of Malware Ground Truth

Malware labels are determined by multiple security engines, often with conflicting decisions. Researchers set thresholds to balance sensitivity and specificity; lower thresholds include borderline software, blurring classification boundaries. In this study, we use a low threshold ( $\nu t = 4$ ) to evaluate performance in this challenging scenario.

Table 6: AUT (F1, 12m) of the Deepdrebin [17] under different regularization methods.

Test Years	DeepDrebin [17]				
	ERM	Early	Dropout	$\ell_2$	Ours
		Stopping			
2015	0.856	0.833	0.859	0.869	0.928
2016	0.808	0.795	0.818	0.822	0.877
2017	0.742	0.736	0.754	0.759	0.815
2018	0.703	0.701	0.726	0.727	0.794
2019	0.682	0.682	0.713	0.704	0.769
2020	0.664	0.668	0.696	0.681	0.732
2021	0.651	0.657	0.686	0.669	0.717
2022	0.628	0.635	0.658	0.641	0.688
2023	0.611	0.617	0.631	0.619	0.665

## 6.2 Comparison to the Regularization Method

ERM-trained models are easy to overfit to unstable features, limiting test set generalization [21]. Regularization methods, such as early stopping,  $\ell_2$  regularization, and dropout, help mitigate this by constraining model parameters [43]. Unlike regularization, invariant learning focuses on stable features under drift scenarios. We compare these regularization methods with our invariant learning framework during the whole test phase (Table 6). For reference, DeepDrebin (ERM) includes no regularization, while DeepDrebin [17] employs dropout with a hyperparameter of 0.2. Table 6 shows dropout improves performance under significant drift, outperforming early stopping and  $\ell_2$  regularization, which fails to capture optimal features. Invariant training consistently outperforms, capturing stable, discriminative features that maintain performance across distributions.

## 6.3 Application Scope of Invariant Learning

Invariant learning enhances a model’s generalization to unseen distributions, but keeping stable to all possible shifts is unrealistic. With significant distribution changes, its effectiveness diminishes, and current research indicates that addressing concept drift typically requires costly model updates, including data labeling, retraining, and redeployment. Additionally, pseudo-label noise from automated labeling can further degrade performance [19]. The true value of a robust malware detector lies in sustaining reliable performance under gradual drifts, extending its lifespan before retraining and reducing the cost of selective updates.

## 7 Conclusion

Android malware detectors suffer performance degradation due to natural distribution changes caused by malware evolution. We identify learnable invariant patterns among malware samples with similar intent, enabling a drift-stable feature space. To address this, we propose a temporal invariant train-

ing framework that organizes samples chronologically and integrates multi-proxy contrastive learning with invariant gradient alignment. Experiments demonstrate improved robustness across feature spaces and drifting scenarios, promoting stable and discriminative representations.

## References

- [1] Kartik Ahuja, Ethan Caballero, Dinghui Zhang, Jean-Christophe Gagnon-Audet, Yoshua Bengio, Ioannis Mitliagkas, and Irina Rish. Invariance principle meets information bottleneck for out-of-distribution generalization. *Advances in Neural Information Processing Systems*, 34:3438–3450, 2021.
- [2] Daniele Angioni, Luca Demetrio, Maura Pintor, and Battista Biggio. Robust machine learning for malware detection over time. *arXiv preprint arXiv:2208.04838*, 2022.
- [3] Martin Arjovsky, Léon Bottou, Ishaan Gulrajani, and David Lopez-Paz. Invariant risk minimization. *arXiv preprint arXiv:1907.02893*, 2019.
- [4] Daniel Arp, Michael Spreitzenbarth, Malte Hubner, Hugo Gascon, Konrad Rieck, and CERT Siemens. Drebin: Effective and explainable detection of android malware in your pocket. In *Ndss*, volume 14, pages 23–26, 2014.
- [5] Federico Barbero, Feargus Pendlebury, Fabio Pierazzi, and Lorenzo Cavallaro. Transcending transcend: Revisiting malware classification in the presence of concept drift. In *2022 IEEE Symposium on Security and Privacy (SP)*, pages 805–823. IEEE, 2022.
- [6] Fabrício Ceschin, Marcus Botacin, Heitor Murilo Gomes, Felipe Pinagé, Luiz S Oliveira, and André Grégio. Fast & furious: On the modelling of malware detection as an evolving data stream. *Expert Systems with Applications*, 212:118590, 2023.
- [7] Meryam Chaieb, Mostafa Anouar Ghorab, and Mohamed Aymen Saied. Detecting android malware: From neural embeddings to hands-on validation with bertroid. *arXiv preprint arXiv:2405.03620*, 2024.
- [8] Yimeng Chen, Ruibin Xiong, Zhi-Ming Ma, and Yanyan Lan. When does group invariant learning survive spurious correlations? *Advances in Neural Information Processing Systems*, 35:7038–7051, 2022.
- [9] Yizheng Chen, Zhoujie Ding, and David Wagner. Continuous learning for android malware detection. In *32nd USENIX Security Symposium (USENIX Security 23)*, pages 1127–1144, 2023.
- [10] Yongqiang Chen, Wei Huang, Kaiwen Zhou, Yatao Bian, Bo Han, and James Cheng. Understanding and improving feature learning for out-of-distribution generalization. *Advances in Neural Information Processing Systems*, 36, 2024.
- [11] Zhi Chen, Zhenning Zhang, Zeliang Kan, Limin Yang, Jacopo Cortellazzi, Feargus Pendlebury, Fabio Pierazzi, Lorenzo Cavallaro, and Gang Wang. Is it overkill? analyzing feature-space concept drift in malware detectors. In *2023 IEEE Security and Privacy Workshops (SPW)*, pages 21–28. IEEE, 2023.
- [12] Theo Chow, Zeliang Kan, Lorenz Linhardt, Lorenzo Cavallaro, Daniel Arp, and Fabio Pierazzi. Drift forensics of malware classifiers. In *Proceedings of the 16th ACM Workshop on Artificial Intelligence and Security*, pages 197–207, 2023.
- [13] Elliot Creager, Jörn-Henrik Jacobsen, and Richard Zemel. Environment inference for invariant learning. In *International Conference on Machine Learning*, pages 2189–2200. PMLR, 2021.
- [14] Elliot Creager, Jörn-Henrik Jacobsen, and Richard Zemel. Environment inference for invariant learning. In *International Conference on Machine Learning*, pages 2189–2200. PMLR, 2021.
- [15] Marco Cuturi. Sinkhorn distances: Lightspeed computation of optimal transport. *Advances in neural information processing systems*, 26, 2013.
- [16] Nadia Daoudi, Kevin Allix, Tegawendé F Bissyandé, and Jacques Klein. Guided retraining to enhance the detection of difficult android malware. In *Proceedings of the 32nd ACM SIGSOFT International Symposium on Software Testing and Analysis*, pages 1131–1143, 2023.
- [17] Kathrin Grosse, Nicolas Papernot, Praveen Manoharan, Michael Backes, and Patrick McDaniel. Adversarial examples for malware detection. In *Computer Security—ESORICS 2017: 22nd European Symposium on Research in Computer Security, Oslo, Norway, September 11–15, 2017, Proceedings, Part II 22*, pages 62–79. Springer, 2017.
- [18] Médéric Hurier, Guillermo Suarez-Tangil, Santanu Kumar Dash, Tegawendé F Bissyandé, Yves Le Traon, Jacques Klein, and Lorenzo Cavallaro. Euphony: harmonious unification of cacophonous anti-virus vendor labels for android malware. In *Proceedings of the 14th International Conference on Mining Software Repositories*, pages 425–435. IEEE Press, 2017.
- [19] Zeliang Kan, Feargus Pendlebury, Fabio Pierazzi, and Lorenzo Cavallaro. Investigating labelless drift adaptation for malware detection. In *Proceedings of the 14th*

- ACM Workshop on Artificial Intelligence and Security*, pages 123–134, 2021.
- [20] David Krueger, Ethan Caballero, Joern-Henrik Jacobsen, Amy Zhang, Jonathan Binas, Dinghuai Zhang, Remi Le Priol, and Aaron Courville. Out-of-distribution generalization via risk extrapolation (rex). In *International conference on machine learning*, pages 5815–5826. PMLR, 2021.
- [21] Jan Kukačka, Vladimir Golkov, and Daniel Cremers. Regularization for deep learning: A taxonomy. *arXiv preprint arXiv:1710.10686*, 2017.
- [22] Jiashuo Liu, Zheyuan Hu, Peng Cui, Bo Li, and Zuo-JunMax Shen. Heterogeneous risk minimization. *arXiv: Learning, arXiv: Learning*, May 2021.
- [23] LydiaT. Liu, Max Simchowitz, and Moritz Hardt. The implicit fairness criterion of unconstrained learning. *arXiv: Learning, arXiv: Learning*, Aug 2018.
- [24] Haodong Lu, Dong Gong, Shuo Wang, Jason Xue, Lina Yao, and Kristen Moore. Learning with mixture of prototypes for out-of-distribution detection. *arXiv preprint arXiv:2402.02653*, 2024.
- [25] Tingting Lu and Junfeng Wang. Domr: Towards deep open-world malware recognition. *IEEE Transactions on Information Forensics and Security*, 2023.
- [26] Kexin Pei, Weichen Li, Qirui Jin, Shuyang Liu, Scott Geng, Lorenzo Cavallaro, Junfeng Yang, and Suman Jana. Exploiting code symmetries for learning program semantics. In *Forty-first International Conference on Machine Learning (Spotlight)*, 2024.
- [27] Feargus Pendlebury, Fabio Pierazzi, Roberto Jordaney, Johannes Kinder, and Lorenzo Cavallaro. {TESSERACT}: Eliminating experimental bias in malware classification across space and time. In *28th USENIX security symposium (USENIX Security 19)*, pages 729–746, 2019.
- [28] Fabio Pierazzi, Feargus Pendlebury, Jacopo Cortellazzi, and Lorenzo Cavallaro. Intriguing properties of adversarial ml attacks in the problem space. In *2020 IEEE Symposium on Security and Privacy (SP)*, pages 1308–1325. IEEE Computer Society, 2020.
- [29] Sachin Ravi and Hugo Larochelle. Optimization as a model for few-shot learning. In *International conference on learning representations*, 2016.
- [30] Megha Srivastava, Tatsunori Hashimoto, and Percy Liang. Robustness to spurious correlations via human annotations. *International Conference on Machine Learning, International Conference on Machine Learning*, Jul 2020.
- [31] Vincent Y. F. Tan, Prashanth L.A., and Krishna Jagannathan. Recent advances in concept drift adaptation methods for deep learning. In *Proceedings of the Thirty-First International Joint Conference on Artificial Intelligence*, Jun 2022.
- [32] Damien Teney, Ehsan Abbasejad, and Anton van den Hengel. Unshuffling data for improved generalization in visual question answering. In *Proceedings of the IEEE/CVF international conference on computer vision*, pages 1417–1427, 2021.
- [33] Yoav Wald, Amir Feder, Daniel Greenfeld, and Uri Shalit. On calibration and out-of-domain generalization. *Advances in neural information processing systems*, 34:2215–2227, 2021.
- [34] Alexander Warnecke, Daniel Arp, Christian Wressnegger, and Konrad Rieck. Evaluating explanation methods for deep learning in security. In *2020 IEEE european symposium on security and privacy (EuroS&P)*, pages 158–174. IEEE, 2020.
- [35] Yueming Wu, Xiaodi Li, Deqing Zou, Wei Yang, Xin Zhang, and Hai Jin. Malscan: Fast market-wide mobile malware scanning by social-network centrality analysis. In *2019 34th IEEE/ACM International Conference on Automated Software Engineering (ASE)*, pages 139–150. IEEE, 2019.
- [36] Ke Xu, Yingjiu Li, Robert Deng, Kai Chen, and Jiayun Xu. Droidevolver: Self-evolving android malware detection system. In *2019 IEEE European Symposium on Security and Privacy (EuroS&P)*, pages 47–62. IEEE, 2019.
- [37] Limin Yang, Wenbo Guo, Qingying Hao, Arridhana Ciprati, Ali Ahmadzadeh, Xinyu Xing, and Gang Wang. {CADE}: Detecting and explaining concept drift samples for security applications. In *30th USENIX Security Symposium (USENIX Security 21)*, pages 2327–2344, 2021.
- [38] Mengyue Yang, Yonggang Zhang, Zhen Fang, Yali Du, Furui Liu, Jean-Francois Ton, Jianhong Wang, and Jun Wang. Invariant learning via probability of sufficient and necessary causes. *Advances in Neural Information Processing Systems*, 36, 2024.
- [39] Shuo Yang, Xinran Zheng, Jinze Li, Jinfeng Xu, Xingjun Wang, and Edith CH Ngai. Recda: Concept drift adaptation with representation enhancement for network intrusion detection. In *Proceedings of the 30th ACM SIGKDD Conference on Knowledge Discovery and Data Mining*, pages 3818–3828, 2024.

- [40] Yuchen Yang, Bo Yuan, Jian Lou, and Zhan Qin. Sccr: Stable malware detection under unknown deployment environment shift by decoupled spurious correlations filtering. *IEEE Transactions on Dependable and Secure Computing*, 2024.
- [41] Xufeng Yao, Yang Bai, Xinyun Zhang, Yuechen Zhang, Qi Sun, Ran Chen, Ruiyu Li, and Bei Yu. Pcl: Proxy-based contrastive learning for domain generalization. In *Proceedings of the IEEE/CVF Conference on Computer Vision and Pattern Recognition*, pages 7097–7107, 2022.
- [42] Yunlong Yu, Zhong Ji, Jungong Han, and Zhongfei Zhang. Episode-based prototype generating network for zero-shot learning. In *Proceedings of the IEEE/CVF conference on computer vision and pattern recognition*, pages 14035–14044, 2020.
- [43] Chiyuan Zhang, Samy Bengio, Moritz Hardt, Benjamin Recht, and Oriol Vinyals. Understanding deep learning (still) requires rethinking generalization. *Communications of the ACM*, 64(3):107–115, 2021.
- [44] Jianyu Zhang, David Lopez-Paz, and Léon Bottou. Rich feature construction for the optimization-generalization dilemma. In *International Conference on Machine Learning*, pages 26397–26411. PMLR, 2022.
- [45] Xiaohan Zhang, Yuan Zhang, Ming Zhong, Daizong Ding, Yinzhi Cao, Yukun Zhang, Mi Zhang, and Min Yang. Enhancing state-of-the-art classifiers with api semantics to detect evolved android malware. In *Proceedings of the 2020 ACM SIGSAC Conference on Computer and Communications Security*, Oct 2020.

## A Dataset Description

### A.1 Sample selection

We construct a dataset spanning 2014 to 2023 using samples from the Androzoo<sup>12</sup> platform, a comprehensive repository aggregating samples from sources such as Google Play, Play-Drone, VirusShare, and AppChina. Each sample’s timestamp corresponds to its submission date on VirusTotal<sup>13</sup>, representing the time it was discovered. The dataset includes a decade of benign and malicious samples, labeled based on VirusTotal analysis from Androzoo. Samples flagged by more than four vendors are classified as malicious. To track malware family evolution, we used Euphony [18] to extract family labels. The dataset comprises 193,978 benign apps and 23,302 malicious apps. To mitigate temporal and spatial biases, we applied the TESSERACT [27] methodology. In our experiments, the training set consists solely of 2014 samples. The dataset’s class

<sup>12</sup><https://androzoo.uni.lu>

<sup>13</sup><https://www.virustotal.com>

distribution, shown in Table A, reflects real-world proportions of benign and malicious samples.

### A.2 Timestamp selection

In Android malware, the dex date is often manipulated or invalid (e.g., many applications display 1980), and the upload date on Androzoo does not necessarily reflect the actual release date of the application. Aware of this issue, we choose to use the observation date of applications on malware detection platforms, such as the “first submission date” provided by VirusTotal, as a more reliable alternative. Due to API access limitations, we selected 10% of newer samples from the dataset (where dex dates are even less reliable) to verify their first submission date on VirusTotal. Comparisons revealed that these dates closely align with the `vt_scan_date` provided by Androzoo. For the full dataset, we therefore approximate the observation date using `vt_scan_date`, referred to as the “application observation date” in the manuscript.

## B Candidate Detectors

Details of each candidate detector are as follows:

**Drebin:** Drebin [4] is a malware detector using binary feature vectors from nine data types (e.g., hardware, API calls, permissions) for linear classification. To align with our framework’s focus on neural network architectures, we include its deep learning variant, DeepDrebin [17], which uses the same feature space but employs a three-layer deep neural network (DNN) for feature extraction and classification.

**Malscan:** Malscan [35] adopts a graph-based feature space, extracting sensitive API calls from APKs and combining four centrality measures (degree, Katz, proximity, and harmonic wave centralities) as features. We concatenate these features according to the optimal method detailed in the paper for detection tasks.

**BERTroid:** BERTroid [7] leverages Android application permission strings, encoding them into dense representations with a BERT-based pre-trained model that captures contextual relationships among permissions. For this study, we use the pooled BERT output as the feature representation for malware detection.

## C Baseline

Details of each baseline are as follows:

**APIGraph:** APIGraph [45] clusters APIs, exceptions, and permissions based on semantic similarities from official documentation, creating an API semantic relationship graph. Similar APIs are represented by a clustered index, forming a stable feature space. From the original method, we derive 2,000 clusters, replacing all features within the same cluster with the corresponding index.



Table 7: Evaluation dataset. The dataset contains 217,280 applications from 2014 to 2023. The malware rate is about 10% per year.

Year	2014	2015	2016	2017	2018	2019	2020	2021	2022	2023	All
Benign	41918	25247	29739	9962	31056	9455	8884	11398	25033	2286	193978
Malicious	5125	2934	3443	1196	3761	1094	1050	1386	3037	276	23302
M+B	47043	28181	32182	11158	34817	10549	9934	12784	28070	2562	217280
M/(M+B)	10.9%	10.4%	10.7%	10.8%	10.4%	10.6%	10.8%	10.8%	10.8%	10.7%	

**Guided Retraining:** Guided Retraining [16] improves malware detection by re-partitioning and retraining on challenging samples. Samples are categorized using the base model’s confusion matrix (TN, TP, FN, FP), and supervised contrastive learning extracts group-specific feature representations, enabling separate processing of easy and difficult samples during inference for better accuracy.

**T-stability:** T-stability [2] introduces t-stability, a metric for SVM models with the Drebin feature space, measuring feature instability via the slope of expected values over time. Then, the above unstable features are constrained to enhance robustness.

As APIGraph and T-stability are tailored to specific feature spaces-APIGraph focusing on API call methods and T-stability on manually selected Drebin [4] features—we use each scheme’s applicable feature space for experiments.

and generalization in the face of distribution drift.

## D Invariant Training Algorithm

The proposed invariant training process is shown in Algorithm 1. This learning framework consists of two phases: discriminative information amplification and unstable information suppression. In Stage 1, the model enhances its ability to learn discriminative features through empirical risk minimization (ERM). Specifically, in Line 6, the classification loss  $\mathcal{L}_{CLS}^e$  is calculated for each environment to ensure correct class separation, and in Line 7, a multi-proxy contrastive (MPC) loss  $\mathcal{L}_{MPC}^e$  is computed to improve the discriminative power among samples. The combined loss for ERM, including the classification and contrastive components, is computed in Line 9, and then the model is updated by backpropagation in Line 10. Stage 2 focuses on suppressing unstable information through invariant training. In Line 14, the optimizer is reset to remove the influence of previous training, while the model parameters from Stage 1 are retained in Line 15 to preserve the learned discriminative capabilities. Line 21 calculates the invariant gradient alignment (IGA) loss  $\mathcal{L}_{IGA}$ . Line 22 calculates overall classification loss for complete samples. The combined invariant risk minimization (IRM) loss is formed in Line 24, integrating the classification, contrastive, and alignment losses and updating the model in Line 25. This two-phase training process enables the model to learn discriminative and stable features, improving robustness

---

**Algorithm 1** Algorithm of Invariant Training

---

**Require:** training dataset containing  $|\mathcal{E}|$  environments  $\mathcal{D}_r$  and each sample  $x$  has a binary classification label  $y_c, c \in [0, 1]$  and an environment label  $y_e, e \in \mathcal{E}$ , batch size  $|\mathcal{B}|$ , predefined number of epochs for stage 1 training  $N$ , hyperparameters  $\alpha$  and  $\beta$  for loss weighting, model  $f$  with encoder network  $\phi$  and predictor  $h$ .

**Ensure:**

```
1: Stage 1: Discriminative Information Amplification
2: for epoch = 1 to  $N$  do
3:   for  $i = 1, \dots, |\mathcal{B}|$  do
4:     for  $e \in \mathcal{E}$  do
5:       select mini-batch of samples  $x_i^e \subseteq \mathcal{B}$ 
6:       calculate classification loss  $\mathcal{L}_{CLS}^e$ 
7:       calculate multi-proxy contrastive loss  $\mathcal{L}_{MPC}^e$ 
8:     end for
9:     obtain loss for empirical risk minimization  $\mathcal{L}_{ERM} = \frac{1}{|\mathcal{E}|} \sum_{e \in \mathcal{E}} \mathcal{L}_{CLS}^e + \alpha \cdot \mathcal{L}_{MPC}^e$ 
10:    update  $f$  by backpropagating  $\mathcal{L}_{ERM}$ 
11:   end for
12: end for
13: Stage 2: Unstable Information Suppression
14: Reset optimizer parameters
15: Continue with model parameters from Stage 1
16: for epoch =  $N + 1$  to TotalEpochs do
17:   for  $i = 1, \dots, |\mathcal{B}|$  do
18:     for  $e \in \mathcal{E}$  do
19:       initialize dummy classifier  $\{s_e = 1.0\}$ 
20:     end for
21:     calculate invariant gradient alignment loss  $\mathcal{L}_{IGA}$ 
22:     obtain classification loss  $\mathcal{L}_{CLS}$ 
23:     obtain multi-proxy contrastive loss  $\mathcal{L}_{MPC}$ 
24:      $\mathcal{L}_{IRM} \leftarrow \mathcal{L}_{CLS} + \alpha \cdot \mathcal{L}_{MPC} + \beta \cdot \mathcal{L}_{IGA}$ 
25:     update  $f$  by backpropagating  $\mathcal{L}_{IRM}$ 
26:   end for
27: end for
```

---